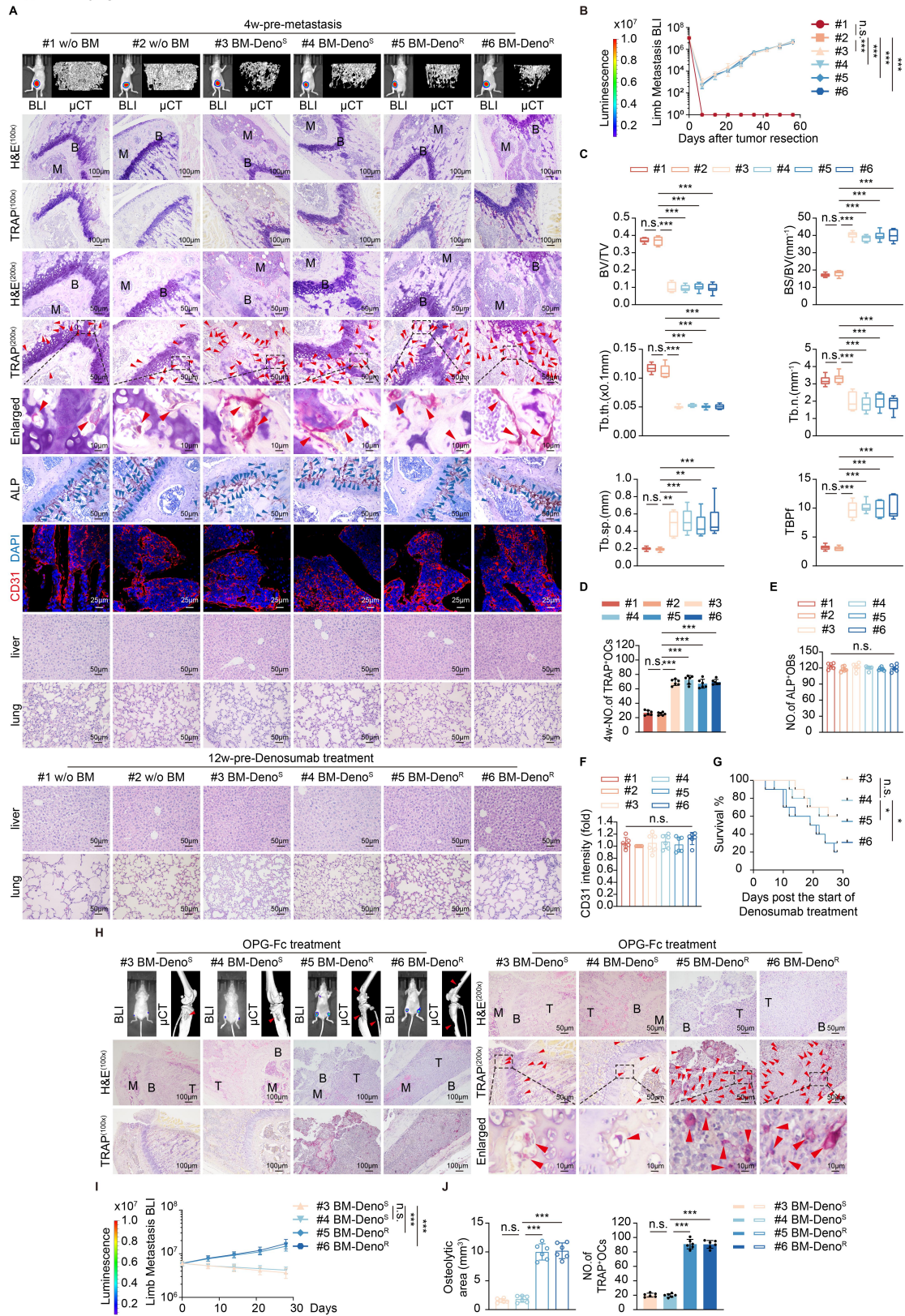


Supplementary figure 1



Supplementary figures and figure legends

Supplementary figure 1. Bone-metastatic breast cancer induces the continuous

## **activation of osteoclasts in the bone microenvironment before the occurrence of bone metastasis**

**A)** Representative BLI images from breast cancer bone metastasis mouse models. representative H&E-stained sections of bone, liver and lung tissues from breast cancer bone metastasis mouse models. Representative  $\mu$ CT images from breast cancer bone metastasis mouse models. Representative TRAP-stained, ALP-stained, CD31 IF-stained sections of bone, tissues from breast cancer bone metastasis mouse models. Scale bar: 100  $\mu$ m, 50  $\mu$ m, 25 $\mu$ m and 10  $\mu$ m.

**B)** Quantification of normalized BLI signals of bone metastases.

**C)** Quantification of the indicated bone parameters and from representative mice (n = 6 per group). BV/TV, bone/tissue volume ratio; BS/TV, bone surface/tissue volume ratio; Tb. n, trabecular number; Tb. sp., trabecular separation; Tb. th., trabecular thickness; TBPf, trabecular bone pattern factor.

**D)** Quantification of the indicated bone parameters and number of TRAP<sup>+</sup> osteoclasts from representative mice

**E)** Quantification of number of ALP<sup>+</sup> osteoblasts.

**F)** Quantification of CD31 fluorescence intensity (angiogenesis).

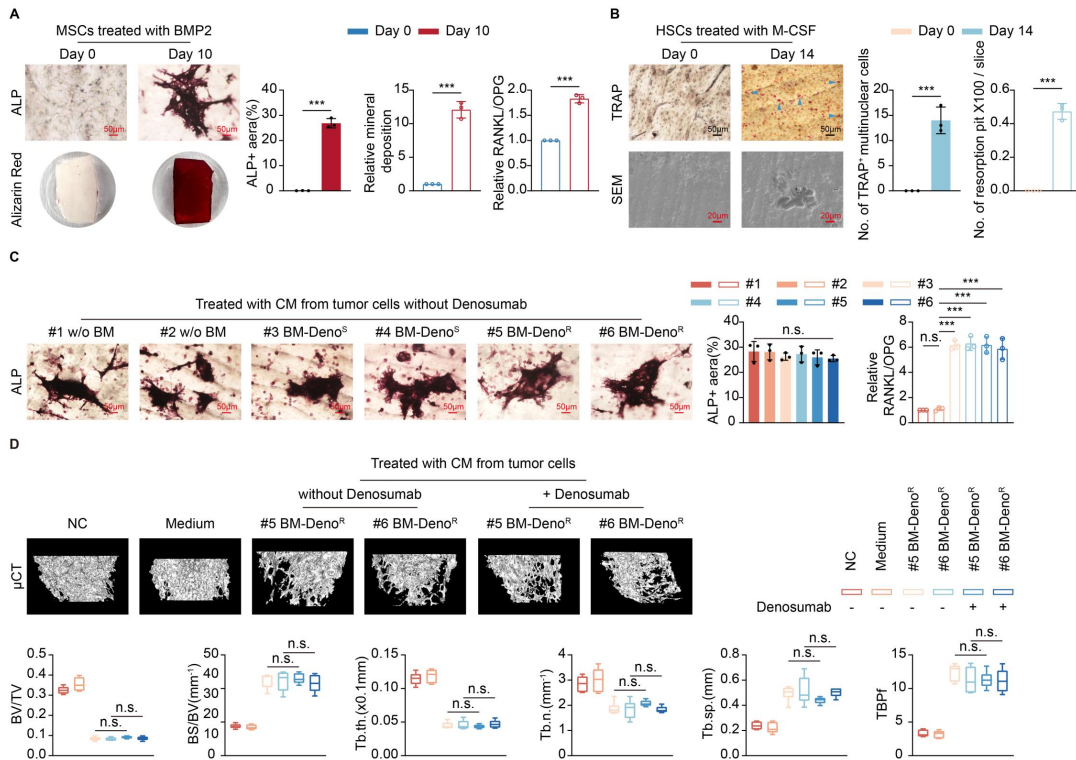
**G)** Kaplan-Meier curves showing prolonged survival in Denosumab-sensitive models (breast cancer bone metastasis mouse model#3-4) versus resistant models (breast cancer bone metastasis mouse model#5-6) after Denosumab therapy initiation.

**H)** BLI images of mice,  $\mu$ CT images of trabecular bone structure in the knee joint, Hematoxylin and eosin (H&E) staining of murine bone tissue, tartrate-resistant acid phosphatase (TRAP) staining. Scale bar: 100  $\mu$ m, 50  $\mu$ m and 10  $\mu$ m.

**I&J)** Quantification of bone parameters, including normalized BLI signals of bone metastases (I),  $\mu$ CT-based osteolytic lesion area and TRAP<sup>+</sup> osteoclast numbers (J) in representative mice (n = 6 per group).

Each error bar represents the mean  $\pm$  SD of 6 independent experiments. Significant differences were determined by one-way ANOVA with Tukey's multiple comparison test. \*  $p < 0.05$ , \*\*  $p < 0.01$ , \*\*\*  $p < 0.001$ .

Supplementary figure 2



**Supplementary figure 2. Differentiation of osteoblasts is not significantly affected by denosumab-resistant breast cancer cells *in vitro*.**

**A)** Left: ALP staining (top) and Alizarin Red S mineralization (bottom) of BMP-treated mesenchymal stem cells (MSCs) at day 0 and day 10. Scale bars: 50  $\mu\text{m}$ . Right: Quantification of ALP<sup>+</sup> area and mineralized matrix deposition (%). RANKL/OPG ratio in conditioned media (CM) from BMP-treated skeletal organoids.

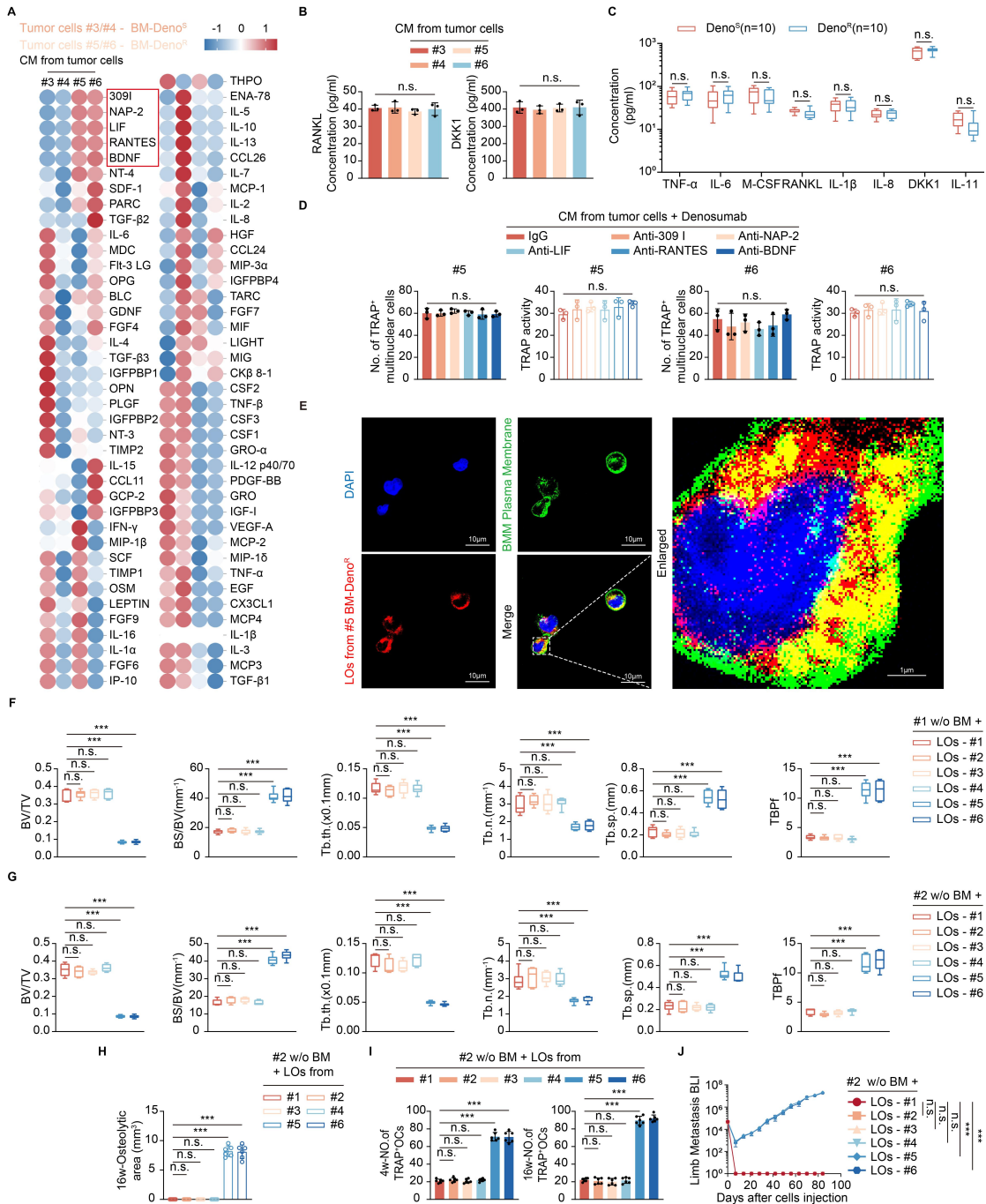
**B)** Left: Representative TRAP-stained osteoclasts (scale bar: 50  $\mu\text{m}$ ) and SEM images of resorption pits (scale bar: 20 $\mu\text{m}$ ). Right: TRAP<sup>+</sup> multinucleated cell counts. Resorption pit numbers per slice.

**C)** Left: ALP staining of bone organoids exposed to conditioned media (CM) from primary breast cancer cells. Scale bars: 50 $\mu\text{m}$ . Right: Quantification of ALP<sup>+</sup> area and mineral deposition (%). RANKL /OPG ratio in CM from BMP-treated organoids.

**D)** Quantification of the indicated bone parameters and from representative mice (n = 6 per group). BV/TV, bone/tissue volume ratio; BS/TV, bone surface/tissue volume ratio; Tb. n, trabecular number; Tb. sp., trabecular separation; Tb. th., trabecular thickness; TBPf, trabecular bone pattern factor.

Each error bar represents the mean  $\pm$  SD of 3 or more independent experiments. Significant differences were determined by one-way ANOVA with Tukey's multiple comparison test. \*  $p < 0.05$ , \*\*  $p < 0.01$ , \*\*\*  $p < 0.001$ .

Supplementary figure 3



**Supplementary figure 3. The uptake of LOs derived from denosumab-resistant breast cancer cells by BMMs leads to RANKL-independent osteoclast activation.**

**A)** Heatmap of a cytokine profiling of conditioned media (CM) from primary breast cancer cells via cytokine array analysis.

**B)** ELISA quantification of soluble RANKL and DKK1 concentrations in CM from primary breast cancer cells.

**C)** Quantification of serum concentrations of classical osteoclast-activating cytokines were quantified by ELISA in denosumab-resistant and -sensitive patients (n = 10 patients/group).

**D)** Quantification of TRAP+ multinucleated osteoclast counts in TRAP staining of BMMs treated with CM pre-incubated with neutralizing antibodies or IgG control and TRAP enzymatic activity in corresponding groups.

**E)** Imaging of mouse BMMs ingesting breast cancer cell-derived LOs by confocal microscopy. BMM membranes were stained with WGA (green), and LOs were labeled with DiL (red). Scale bars: 10 $\mu$ m and 1 $\mu$ m.

**F)** BV/TV, bone/tissue volume ratio; BS/TV, bone surface/ tissue volume ratio; Tb. n, trabecular number; Tb. sp., trabecular separation; Tb. th., trabecular thickness; TBPf, trabecular bone pattern factor.

**G)** Quantification of the indicated bone parameters and number of TRAP+-osteoclasts/ALP+-osteoblasts from representative mice (n = 6 per group). BV/TV, bone/tissue volume ratio; BS/TV, bone surface/tissue volume ratio; Tb. n, trabecular number; Tb. sp., trabecular separation; Tb. th., trabecular thickness; TBPf, trabecular bone pattern factor.

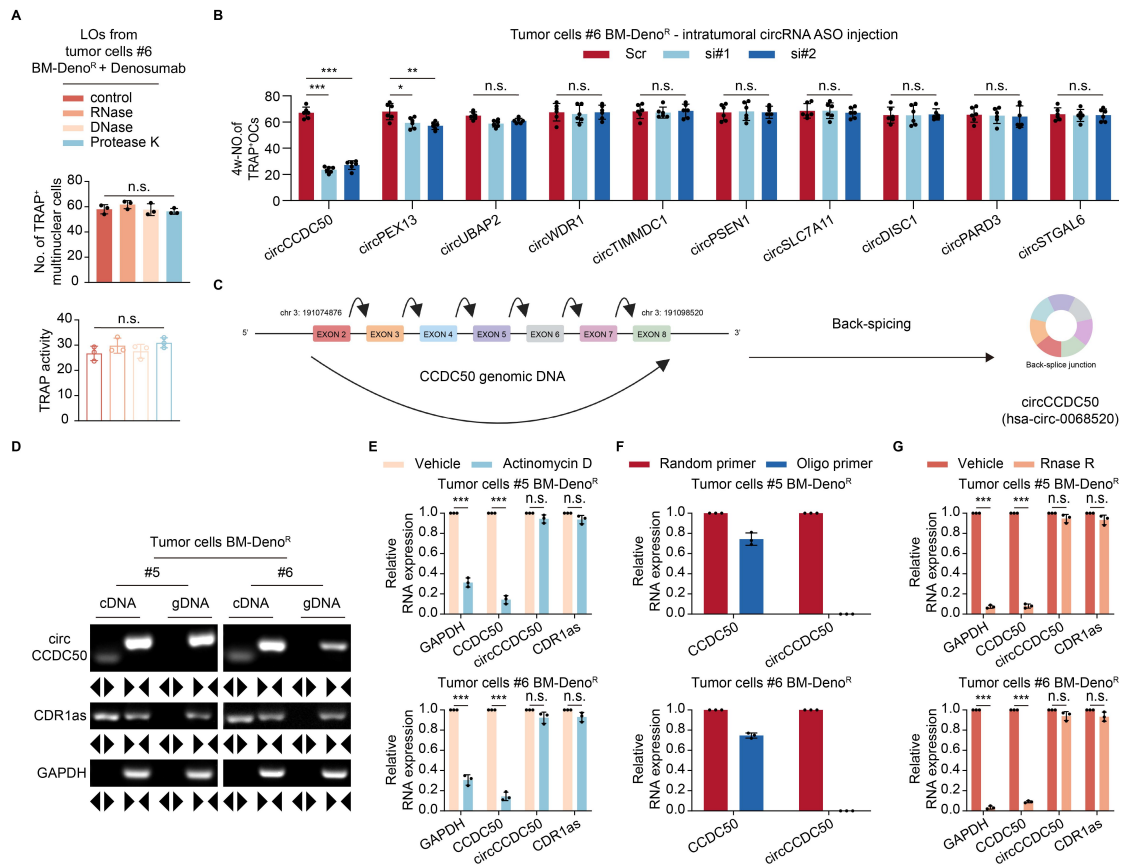
**H)** Quantification of osteolytic area.

**I)** Quantification of tartrate-resistant acid phosphatase (TRAP) staining (scale bar: 50  $\mu$ m) .

**J)** BLI images of breast cancer cells and quantification of BLI imaging of bone microenvironment colonization by non-metastatic primary breast cancer cells #2 following LO treatment.

Each error bar represents the mean  $\pm$  SD of 3 or more independent experiments. Significant differences were determined by one-way ANOVA with Tukey's multiple comparison test. \*  $p < 0.05$ , \*\*  $p < 0.01$ , \*\*\*  $p < 0.001$ .

Supplementary figure 4



Supplementary figure 4. CircCCDC50 has a circular structure.

**A)** Quantification of TRAP<sup>+</sup> multinucleated cells (upper) and TRAP activity (lower).

**B)** TRAP<sup>+</sup> multinucleated osteoclast counts in bone tissues of breast cancer bone metastasis models (#5, #6) treated with circRNA-targeting siRNA or non-targeting siRNA control.

**C)** Schematic illustration of circCCDC50 formation via the circularization of exons 2-3-4-5-6-7-8 in CCDC50 gene. The back-splice junction sequence of circCCDC50 was validated by Sanger sequencing.

**D)** The existence of circCCDC50 was confirmed by RT-PCR and gel electrophoresis in primary tumor cells #5, 6 using the divergent and convergent primers, respectively. Divergent primers amplified circCCDC50 in cDNA but not genomic DNA (gDNA), along with CDR1as as a positive control, GAPDH as a negative control.

**E)** qRT-PCR analysis of stability of circ CCDC50 and linear CCDC50 in the Actinomycin D-treated primary tumor cells #5, 6, along with CDR1as as a positive control, GAPDH as a negative control.

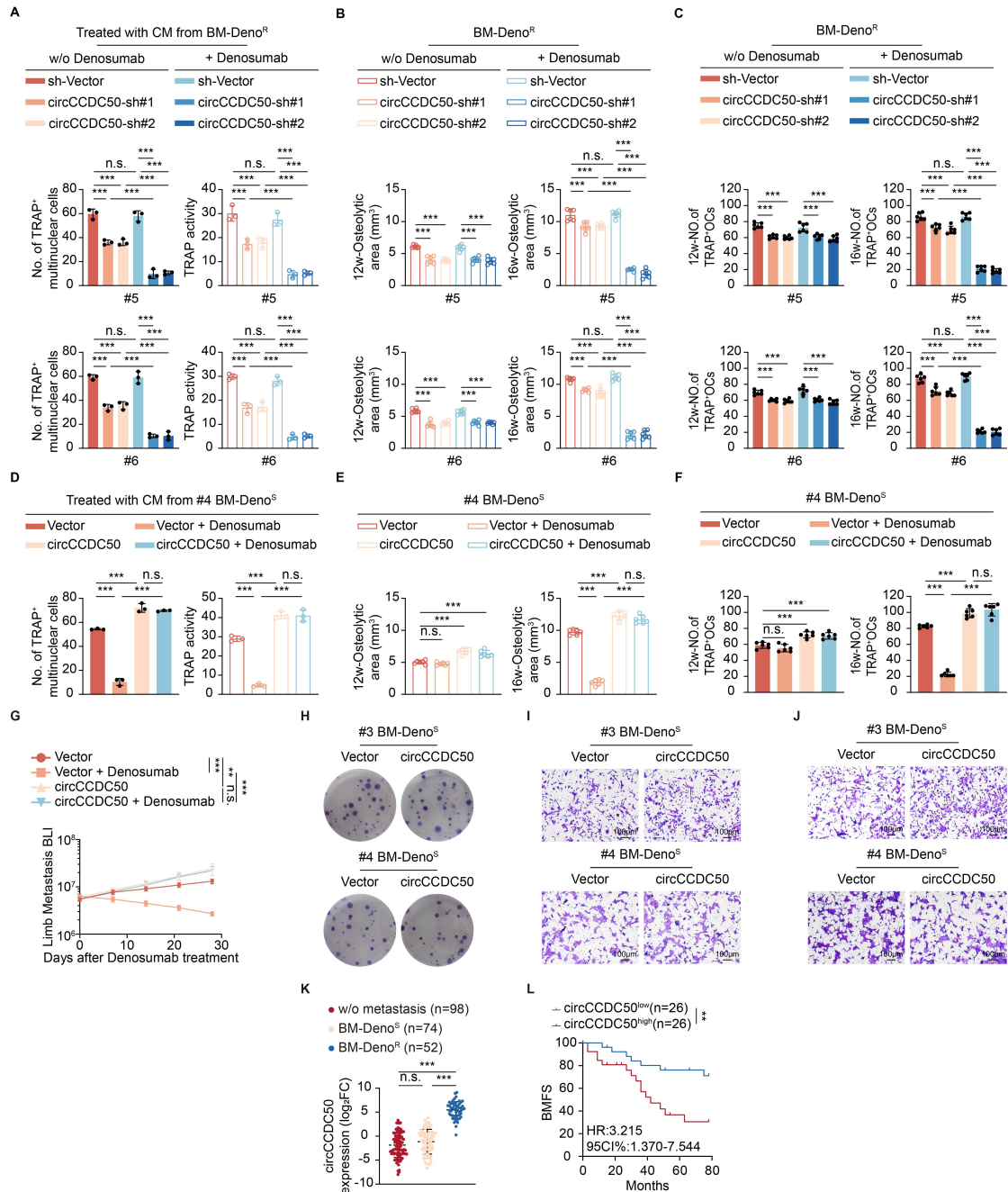
**F)** qRT-PCR analysis of expression of circCCDC50 and linear CCDC50 using random hexamer or oligo(dT)18 primers in primary tumor cells #5, 6. GAPDH served as a loading

control.

**G)** qRT-PCR analysis of stability of circ CCDC50 and linear CCDC50 in the RNase R-treated primary tumor cells #5, 6, along with CDR1as as a positive control, GAPDH as a negative control.

Each error bar represents the mean  $\pm$  SD of 3 or more independent experiments. Significant differences were determined by one-way ANOVA with Tukey's multiple comparison test. \*  $p < 0.05$ , \*\*  $p < 0.01$ , \*\*\*  $p < 0.001$ .

Supplementary figure 5



**Supplementary figure 5. Overexpression of circCCDC50 promotes bone metastasis of denosumab-resistant breast cancer *in vivo*.**

**A)** Quantification of TRAP<sup>+</sup> multinucleated osteoclasts (OCs) in bone marrow-derived macrophages (BMMs) treated with conditioned media (CM) from primary breast cancer cells with different circCCDC50 expression, with or without Denosumab and TRAP enzymatic activity in corresponding groups.

**B, C)** Quantification of osteolytic area (B) and TRAP<sup>+</sup> OCs (C) in breast cancer models implanted into breast cancer cells #5 and #6 with different circCCDC50 expression, treated with or without Denosumab.

**D)** Quantification of TRAP+ multinucleated osteoclasts (OCs) in bone marrow-derived macrophages (BMMs) treated with conditioned media (CM) from breast cancer cells with different circCCDC50 expression, with or without Denosumab and TRAP enzymatic activity in corresponding groups.

**E, F)** Quantification of osteolytic area (E) and TRAP+ OCs (F) in breast cancer models implanted into breast cancer cells #6 with different circCCDC50 expression, treated with or without Denosumab.

**G)** Quantification of normalized BLI signals of mice.

**H)** Representative images of colony formation assays in breast cancer cells #3 and #4 with or without circCCDC50 overexpression.

**I)** Representative images of Transwell migration assays in breast cancer cells #3 and #4 with or without circCCDC50 overexpression.

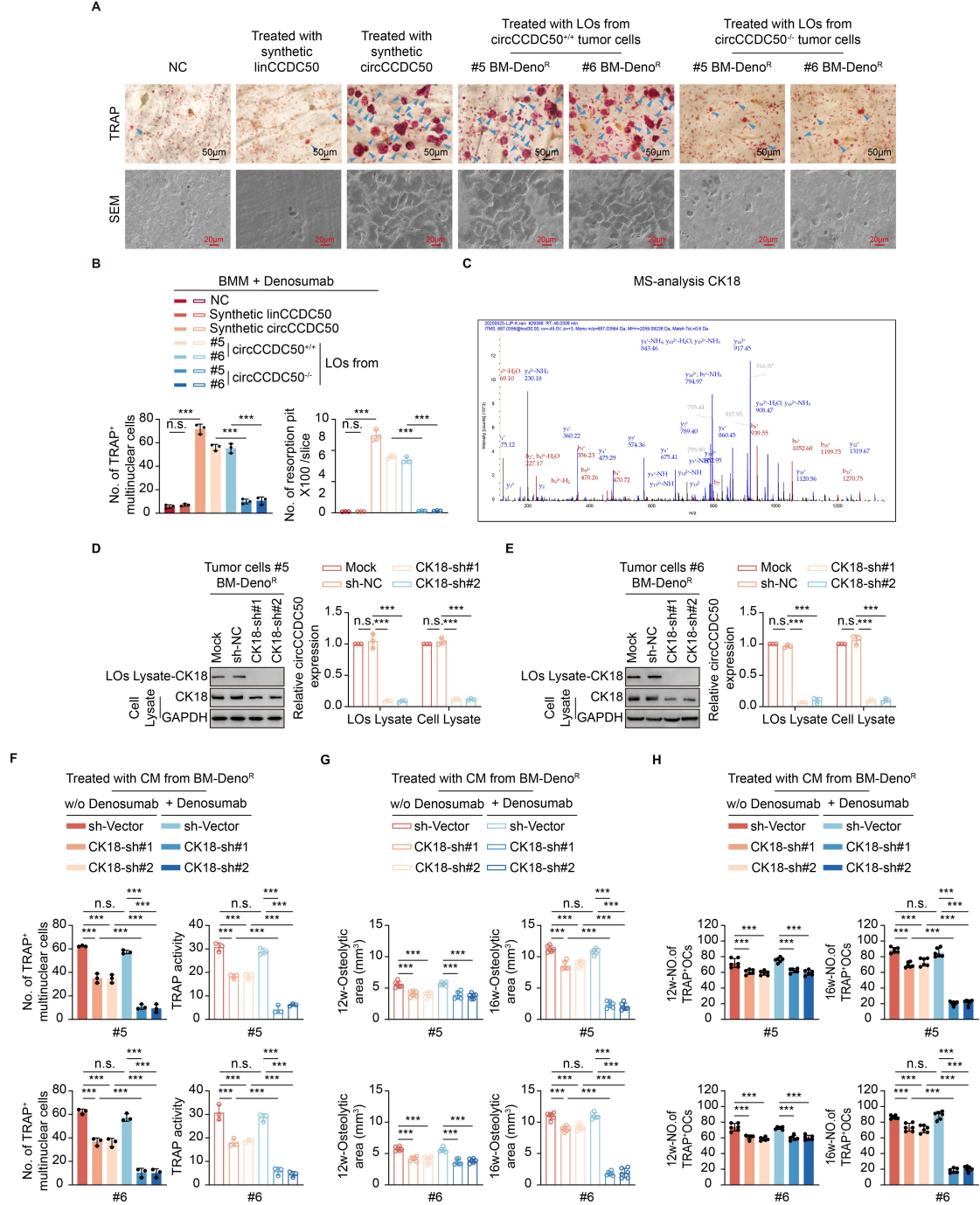
**J)** Representative images of Matrigel-coated Transwell invasion assays in breast cancer cells #3 and #4 with or without circCCDC50 overexpression.

**K)** Analysis of plasma circCCDC50 levels in three patient cohorts: non-metastatic breast cancer (n=98); Denosumab-sensitive bone metastasis (n=74); and Denosumab-resistant bone metastasis (n=51).

**L)** Survival analysis of plasma circCCDC50 levels and patient BMFS.

Each error bar represents the mean  $\pm$  SD of 3 or more independent experiments. Significant differences were determined by one-way ANOVA with Tukey's multiple comparison test. \*  $p < 0.05$ , \*\*  $p < 0.01$ , \*\*\*  $p < 0.001$ .

Supplementary figure 6



**Supplementary figure 6. circCCDC50 knockout leads to a significant impairment in osteoclast activation by denosumab-resistant breast cancer cells *in vitro*.**

**A)** Representative TRAP-stained images (scale bar: 50µm) and SEM micrographs (scale bar: 20µm) of skeletal organoid models treated with Denosumab in combination with either synthetic linear CCDC50 mRNA, circCCDC50, or conditioned medium.

**B)** Quantification of TRAP<sup>+</sup> multinucleated cells (left) and resorption pits per section (right) in treated skeletal organoid models.

**C)** Proteins co-precipitated with circCCDC50 were identified via ChIRP-MS. CK18 exhibited

high binding affinity.

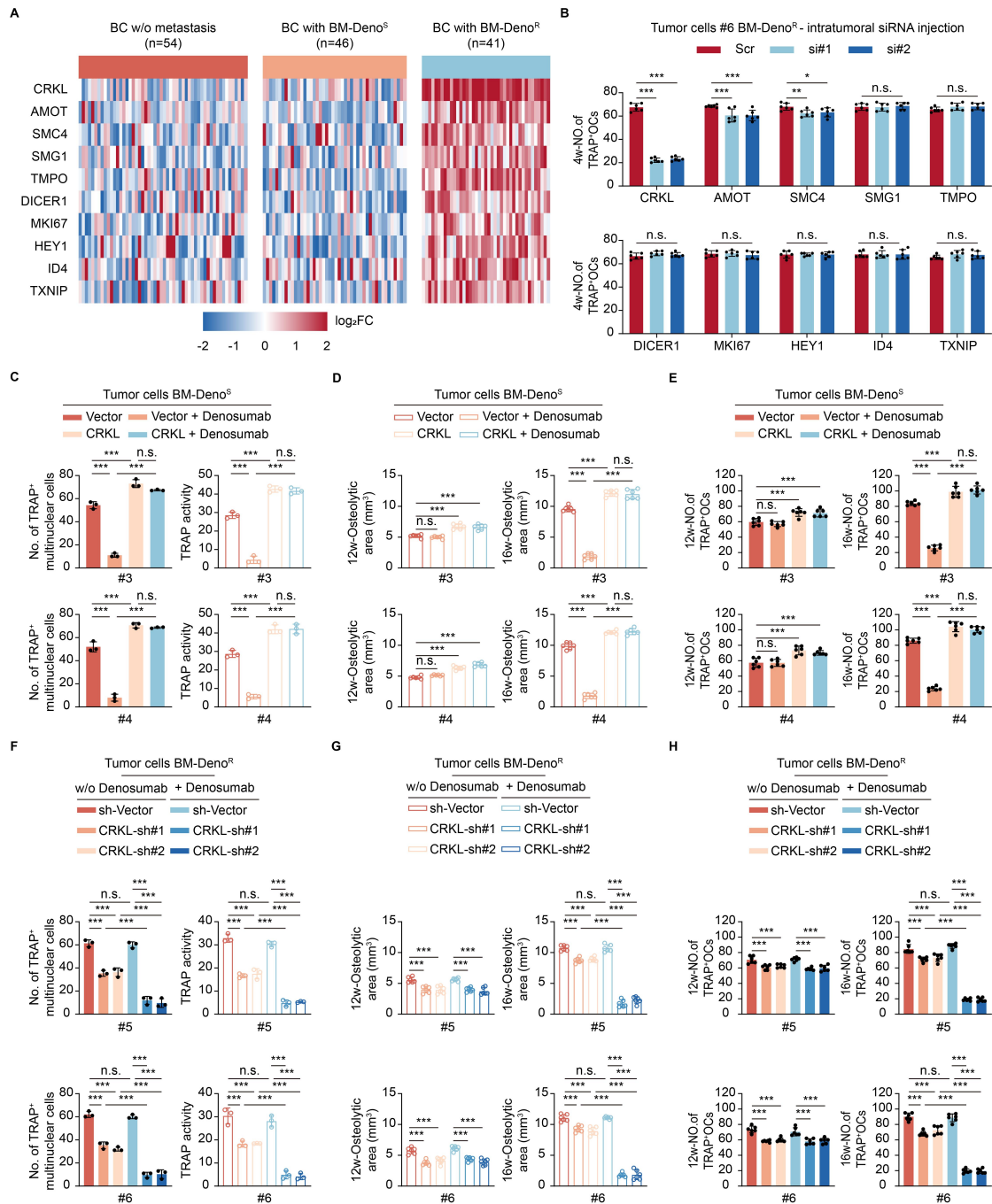
**D&E)** qRT-PCR detection of circCCDC50 levels in cell lysates and LO lysates of primary tumor cells #5(D) and #6(E).

**F)** Quantification of TRAP<sup>+</sup> multinucleated osteoclasts (OCs) in bone marrow-derived macrophages (BMMs) treated with conditioned media (CM) from breast cancer cells with different CK18 expression, with or without Denosumab and TRAP enzymatic activity in corresponding groups.

**G&H)** Quantification of osteolytic area (G) and TRAP<sup>+</sup> OCs (H) in breast cancer models implanted into breast cancer cells #5 or #6 with different CK18 expression, treated with or without Denosumab.

Each error bar represents the mean  $\pm$  SD of 3 or more independent experiments. Significant differences were determined by one-way ANOVA with Tukey's multiple comparison test. \*  $p < 0.05$ , \*\*  $p < 0.01$ , \*\*\*  $p < 0.001$ .

Supplementary figure 7



Supplementary figure 7. Overexpression of CRKL promotes bone metastasis of denosumab-resistant breast cancer *in vitro* and *in vivo*.

A) Heatmap of RT-qPCR validation results for differentially expressed genes (DEGs) identified through transcriptomic sequencing and pathway enrichment analysis.

B) TRAP<sup>+</sup> multinucleated osteoclast counts in bone tissues of breast cancer models #6 treated with dysregulated mRNAs -targeting siRNA or non-targeting siRNA control (n = 6 mice/group).

C) Quantification of TRAP<sup>+</sup> multinucleated osteoclasts (OCs) in bone marrow-derived

macrophages (BMMs) treated with conditioned media (CM) from primary breast cancer cells with different CRKL expression, with or without Denosumab and TRAP enzymatic activity in corresponding groups.

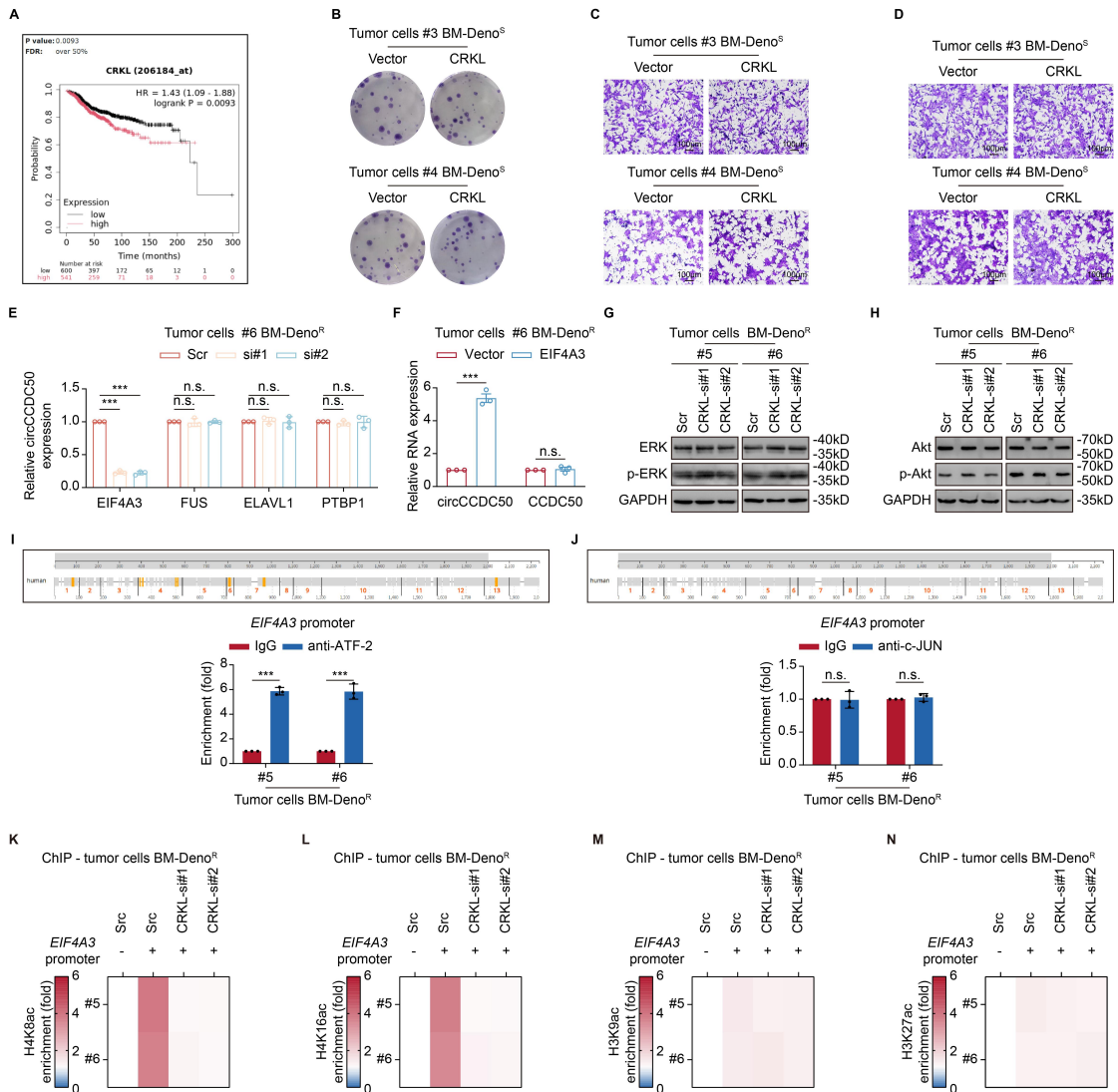
**D, E**) Quantification of osteolytic area (D) and TRAP<sup>+</sup> OCs (E) in breast cancer models implanted into breast cancer cells #5 and #6 with different CRKL expression, treated with or without Denosumab.

**F**) Quantification of TRAP<sup>+</sup> multinucleated osteoclasts (OCs) in bone marrow-derived macrophages (BMMs) treated with conditioned media (CM) from primary breast cancer cells with different CRKL expression, with or without Denosumab and TRAP enzymatic activity in corresponding groups.

**G, H**) Quantification of osteolytic area (G) and TRAP<sup>+</sup> OCs (H) in breast cancer models implanted into breast cancer cells #5 and #6 with different CRKL expression, treated with or without Denosumab.

Each error bar represents the mean  $\pm$  SD of 3 or more independent experiments. Significant differences were determined by one-way ANOVA with Tukey's multiple comparison test. \*  $p < 0.05$ , \*\*  $p < 0.01$ , \*\*\*  $p < 0.001$ .

Supplementary figure 8



**Supplementary figure 8. Binding of ATF-2 to the EIF4A3 promoter induces histone H3 and H4 acetylation.**

**A)** Survival analysis of CRKL expression and patient prognosis based on the Kaplan–Meier plotter database.

**B)** Representative images of colony formation assays in breast cancer cells #3 and #4 with or without CRKL overexpression.

**C)** Representative images of Transwell migration assays in breast cancer cells #3 and #4 with or without CRKL overexpression.

**D)** Representative images of Matrigel-coated Transwell invasion assays in breast cancer cells #3 and #4 with or without CRKL overexpression.

**E)** Real-time PCR analysis of circCCDC50 expression in primary tumor cells #6. GAPDH served as a loading control.

**F)** Real-time PCR analysis of circCCDC50 and CCDC50 expression in

EIF4A3-overexpressing and control tumor cells #6. GAPDH served as a loading control.

**G)** Immunoblots of phosphorylated ERK (p-ERK) and total ERK (t-ERK) in tumor cells transfected with CRKL-targeting siRNA (si-CRKL) or scrambled siRNA control (si-Ctrl). GAPDH served as a loading control.

**H)** Immunoblots of phosphorylated Akt (p-Akt) and total Akt (t-Akt) in tumor cells transfected with CRKL-targeting siRNA (si-CRKL) or scrambled siRNA control (si-Ctrl). GAPDH served as a loading control.

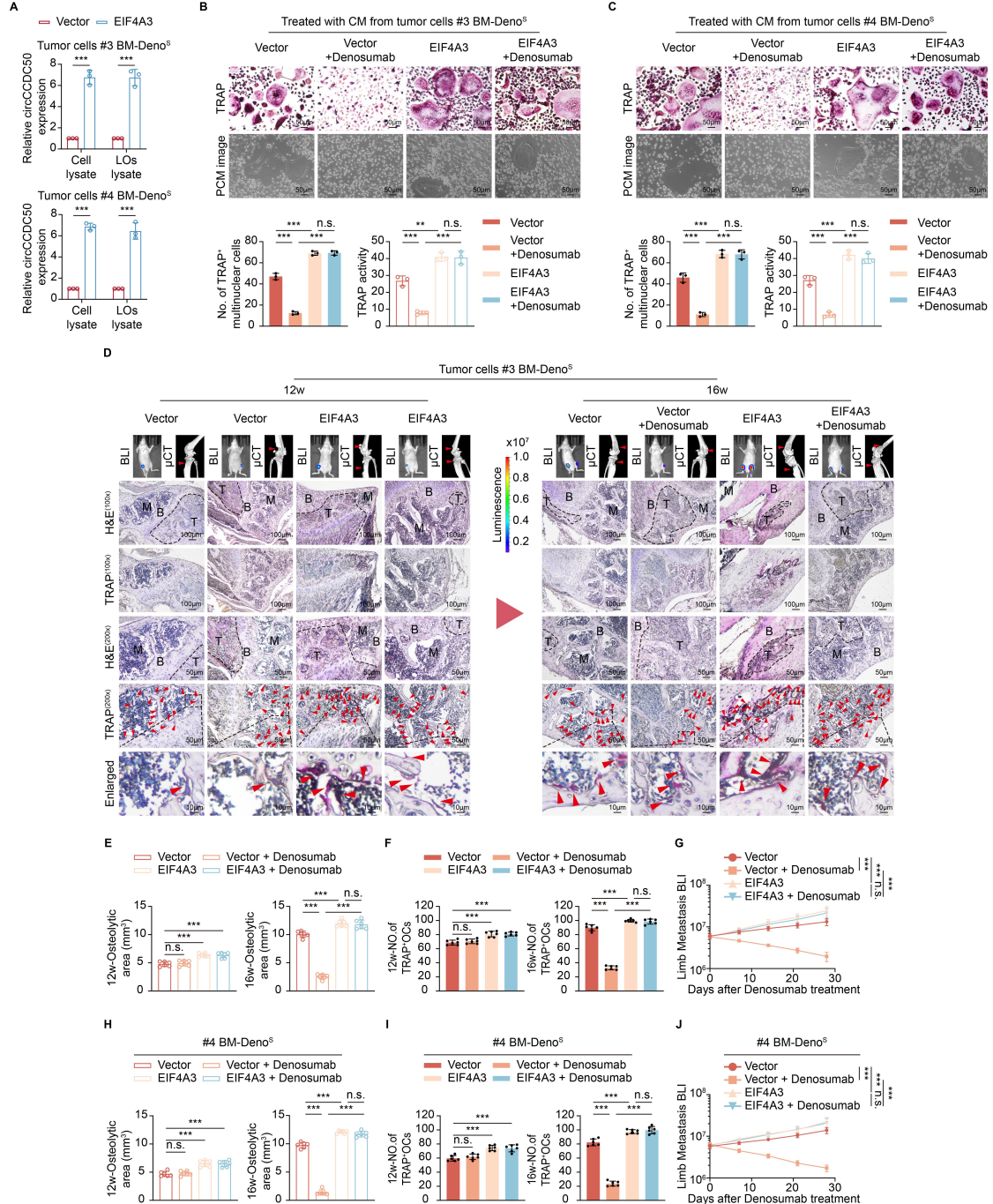
**I)** Bioinformatically predicted ATF-2 binding sites on the NFATc1 promoter and validated by ChIP-qPCR.

**J)** Bioinformatically predicted ATF-2:c-JUN heterodimer binding sites on the NFATc1 promoter and validated by ChIP-qPCR.

**K-N)** H4K8ac (K), H4K16ac (L), H3K9ac (M), and H3K27ac (N) enrichment at the EIF4A3 promoter region was elevated in resistant cells by ChIP-qPCR. EIF4A3 promoter (+) indicates the H4K8ac, H4K16ac, H3K9ac, and H3K27ac enrichment at the EIF4A3 promoter region; EIF4A3 promoter (-) indicates the enrichment at a negative control region.

Each error bar represents the mean  $\pm$  SD of 3 independent experiments. Significant differences were determined by one-way ANOVA with Tukey's multiple comparison test. \*  $p < 0.05$ , \*\*  $p < 0.01$ , \*\*\*  $p < 0.001$ .

Supplementary figure 9



**Supplementary figure 9. Overexpression of EIF4A3 promotes bone metastasis of denosumab-resistant breast cancer *in vitro* and *in vivo*.**

**A)** qPCR analysis of EIF4A3 mRNA expression in breast cancer cells with or without EIF4A3 overexpression and LOs derived from them.

**B)** Quantification of TRAP+ multinucleated osteoclasts (OCs) in bone marrow-derived macrophages (BMMs) treated with conditioned media (CM) from primary breast cancer cells #3 BM-Deno<sup>S</sup> with different EIF4A3 expression, with or without Denosumab and TRAP enzymatic activity in corresponding groups.

**C)** Quantification of TRAP+ multinucleated osteoclasts (OCs) in bone marrow-derived

macrophages (BMMs) treated with conditioned media (CM) from primary breast cancer cells #4 BM-Deno<sup>S</sup> with different EIF4A3 expression, with or without Denosumab and TRAP enzymatic activity in corresponding groups.

**D)** BLI images and  $\mu$ CT scans of bone tissues from breast cancer models, Representative images of hematoxylin and eosin (H&E) staining, tartrate-resistant acid phosphatase (TRAP) staining. Scale bar: 100  $\mu$ m (100x), 50  $\mu$ m (200x) and 10  $\mu$ m (Enlarged).

**E)** Quantitative analysis of osteolytic lesion area via  $\mu$ CT in mice (n = 6 per group).

**F)** Quantitative analysis of TRAP<sup>+</sup> multinucleated cell counts per field in mice (n = 6 per group).

**G)** Quantification of normalized BLI signals of mice (n = 6 per group).

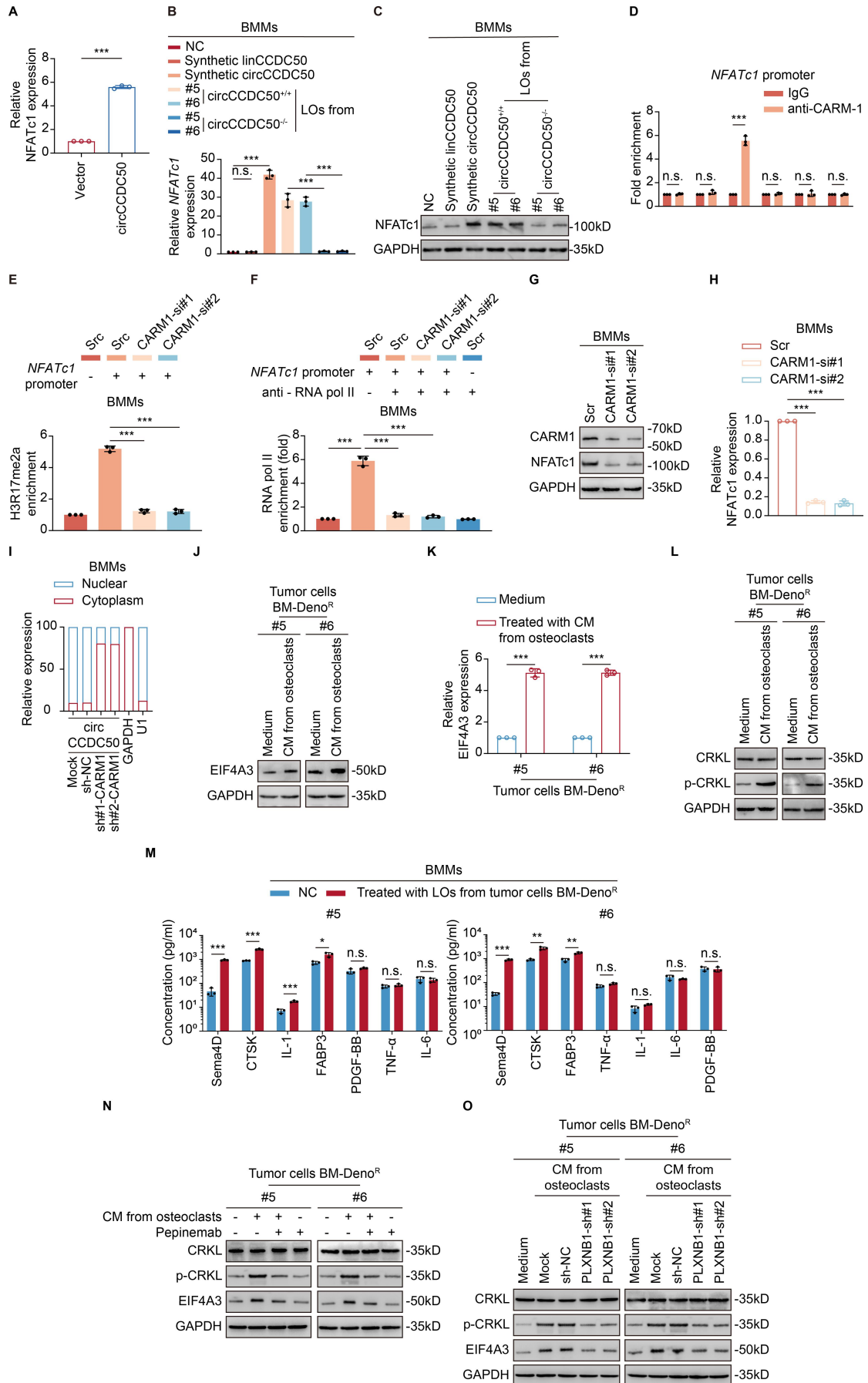
**H)** Quantitative analysis of osteolytic lesion area via  $\mu$ CT in mice (n = 6 per group).

**I)** Quantitative analysis of TRAP<sup>+</sup> multinucleated cell counts per field in mice (n = 6 per group).

**J)** Quantification of normalized BLI signals of mice (n = 6 per group).

Each error bar represents the mean  $\pm$  SD of 3 or more independent experiments. Significant differences were determined by one-way ANOVA with Tukey's multiple comparison test. \*  $p < 0.05$ , \*\*  $p < 0.01$ , \*\*\*  $p < 0.001$ .

Supplementary figure 10



Supplementary figure 10. SEMA4D secreted by osteoclasts upregulates EIF4A3

**expression in denosumab-resistant breast cancer cells.**

**A)** qRT-PCR analysis of NFATc1 expression in BMMs with or without circCCDC50 overexpression.

**B)** qPCR analysis of NFATc1 mRNA expression in mice BMMs treated with Denosumab in combination with synthetic linear CCDC50 mRNA, circCCDC50, or conditioned medium.

**C)** Western blot analysis of NFATc1 protein expression in mice BMMs treated with Denosumab in combination with synthetic linear CCDC50 mRNA, circCCDC50, or conditioned medium.

**D)** ChIP-qPCR validation of CARM1 binding to the NFATc1 promoter.

**E)** H3R17me2a enrichment at the NFATc1 promoter region was elevated in BMMs with or without CARM1 knockdown by ChIP-qPCR. NFATc1 promoter (+) indicates the H3R17me2a enrichment at the NFATc1 promoter region; NFATc1 promoter (-) indicates the enrichment at a negative control region.

**F)** RNA pol II occupancy at the NFATc1 promoter was elevated in BMMs with or without CARM1 knockdown by ChIP-qPCR. NFATc1 promoter (+) indicates the RNA pol II enrichment at the NFATc1 promoter region; NFATc1 promoter (-) indicates the RNA pol II enrichment at a negative control region. anti-RNA pol II (+) indicates ChIP with an anti-RNA polymerase II antibody; anti-RNA pol II (-) indicates ChIP with a control IgG antibody.

**G)** Western-blot analysis of NFATc1 protein in CARM1-knockdown BMMs

**H)** qRT-PCR analysis of NFATc1 mRNA in CARM1-knockdown BMMs.

**I)** Nuclear-cytoplasmic fractionation assay to assess circCCDC50 distribution in CARM1-knockdown BMMs.

**J)** Immunoprecipitation analysis of EIF4A3 expression in primary breast cancer cells (#5, #6) treated with osteoclast-conditioned medium (CM).

**K)** qRT-PCR analysis of EIF4A3 mRNA in CM-treated breast cancer cells.

**L)** Immunoprecipitation analysis of CRKL phosphorylation in CM-treated breast cancer cells.

**M)** ELISA quantification of cytokine secretion in osteoclasts treated with LOs from breast cancer cells (#5, #6).

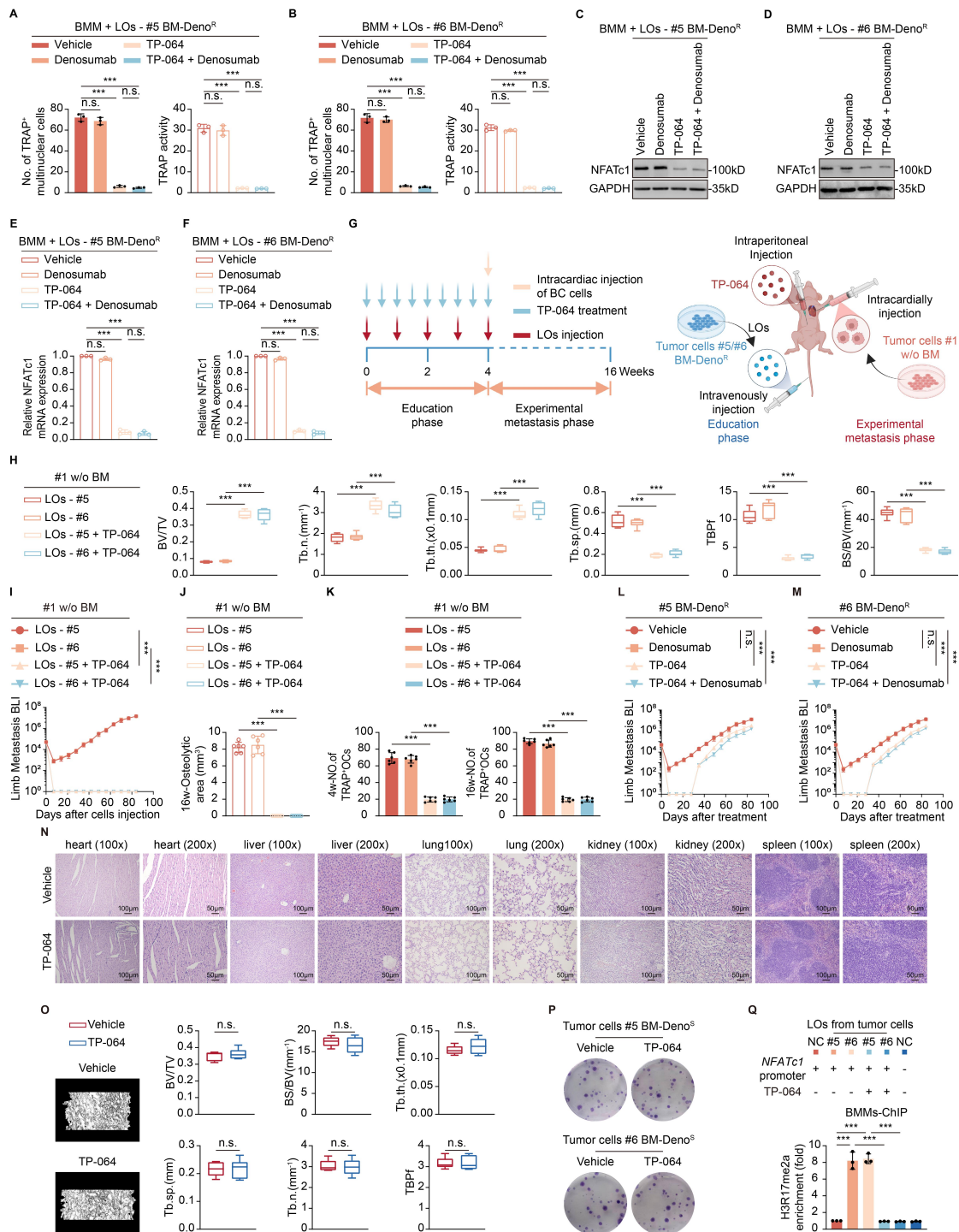
**N)** Western-blot analysis of CRKL phosphorylation and EIF4A3 levels in breast cancer cells treated with CM  $\pm$  Pepinemab (SEMA4D inhibitor).

**O)** Western-blot analysis of CRKL phosphorylation and EIF4A3 levels in

PLXNB1-knockdown breast cancer cells treated with CM.

Each error bar represents the mean  $\pm$  SD of 3 independent experiments. Significant differences were determined by one-way ANOVA with Tukey's multiple comparison test. \*  $p < 0.05$ , \*\*  $p < 0.01$ , \*\*\*  $p < 0.001$ .

Supplementary figure 11



Supplementary figure 11. Administration of TP-064 inhibits the colonization of

**denosumab-resistant breast cancer cells in the bone microenvironment *in vivo*.**

**A, B)** TRAP<sup>+</sup> multinucleated cell counts in BMMs exposed to CM from resistant cells #5 (A) and #6 (B) treated with denosumab, TP-064, or combination therapy. TRAP enzymatic activity (nmol pNP/min/mg protein) in corresponding groups.

**C, D)** NFATc1 protein levels were evaluated in denosumab-resistant primary breast cancer cell lines #5 (C), #6 (D), treated with or without TP-064. GAPDH served as a loading control.

**E, F)** NFATc1 relative mRNA expression were evaluated in denosumab-resistant primary breast cancer cell lines #5 (E), #6 (F), treated with or without TP-064 by qRT-PCR.

**G)** Schematic overview of the pre-metastatic niche education and experimental metastasis mouse models.

**H)** Quantification of the indicated bone parameters and from representative mice (n = 6 per group). BV/TV, bone/tissue volume ratio; BS/TV, bone surface/tissue volume ratio; Tb. n, trabecular number; Tb. sp., trabecular separation; Tb. th., trabecular thickness; TBPf, trabecular bone pattern factor.

**I)** Quantification of normalized BLI signals in animal models with different treatments.

**J)**  $\mu$ CT-based analysis of osteolytic lesion area in bone tissues of breast cancer bone metastasis mouse models treated with indicated therapies.

**K)** Quantification of TRAP<sup>+</sup> multinucleated osteoclasts per field in bone tissues of breast cancer bone metastasis mouse models treated with indicated therapies.

**L)** Quantification of normalized BLI signals in #5 animal models with different treatments.

**M)** Quantification of normalized BLI signals in #6 animal models with different treatments.

**O)** Left: Representative  $\mu$ CT images of trabecular bone from humanized NCG-hairless mice treated with or without TP-064. Right: Quantification of the indicated bone parameters and from representative mice (n = 6 per group). BV/TV, bone/tissue volume ratio; BS/TV, bone surface/tissue volume ratio; Tb. n, trabecular number; Tb. sp., trabecular separation; Tb. th., trabecular thickness; TBPf, trabecular bone pattern factor.

**P)** Colony formation assay of Denosumab-resistant ER-positive breast cancer cells treated with or without 0.1  $\mu$ M TP-064.

**Q)** H3R17me2a enrichment at the NFATc1 promoter region was elevated in BMMs derived from NCG-hairless mice following treatment with or without LOs and with or without TP-064 by ChIP-qPCR. NFATc1 promoter (+) indicates the H3R17me2a enrichment at the NFATc1 promoter region; NFATc1 promoter (-) indicates the enrichment at a negative control

region. TP-064 (+) indicates NCG-hairless mice treated with TP-064; TP-064 (-) indicates NCG-hairless mice treated without TP-064.

Each error bar represents the mean  $\pm$  SD of 3 or more independent experiments. Significant differences were determined by one-way ANOVA with Tukey's multiple comparison test. \*  $p < 0.05$ , \*\*  $p < 0.01$ , \*\*\*  $p < 0.001$ .

## Supplementary table

**Supplementary Table 1. Baseline and characteristics of patients.**

<b>Patients number</b>	1	2	3	4	5	6
<b>Age, years</b>	56	61	59	57	63	61
<b>ER receptor status</b>	+	+	+	+	+	+
<b>PR receptor status</b>	+	+	+	+	+	+
<b>HER2 status</b>	IHC 1+	IHC 0	IHC 1+	IHC 1+	IHC 1+	IHC 0
<b>Ki67 expression</b>	10%	15%	5%	15%	10%	10%
<b>Molecular subtype</b>	Luminal A	Luminal A	Luminal A	Luminal A	Luminal A	Luminal A
<b>Clinically TNM stage</b>	IV	IV	IV	IV	IV	IV
<b>Bone metastasis</b>	-	-	+	+	+	+
<b>Visceral metastasis</b>	-	-	-	-	-	-

HR: hormone receptor. PR: Progesterone Receptor. HER2: human epidermal growth factor receptor 2. IHC: immunochemistry.